Analysis of Time Optimal Control Strategies for Electrically Excited Synchronous Machines Using Dynamic Optimization

Leonard Geier
Elektrotechnisches Institut (ETI)
Karlsruhe Institute of Technology (KIT)
Karlsruhe, Germany
leonard.geier@kit.edu

Johannes Stoß
Elektrotechnisches Institut (ETI)
Karlsruhe Institute of Technology (KIT)
Karlsruhe, Germany
johannes.stoss@kit.edu

Dr.-Ing. Andreas Liske
Elektrotechnisches Institut (ETI)
Karlsruhe Institute of Technology (KIT)
Karlsruhe, Germany
andreas.liske@kit.edu

Prof. Dr.-Ing. Marc Hiller
Elektrotechnisches Institut (ETI)
Karlsruhe Institute of Technology (KIT)
Karlsruhe, Germany
marc.hiller@kit.edu

***Abstract*—In this work a systematic analysis is conducted to identify the maximum possible dynamics regarding torque and rotor flux change in electrically excited synchronous machines (EESM). For this, a numerical approach to solve the nonlinear dynamic optimization problem is presented that does not require simplifications of the machine dynamics and can be applied in the whole operating region. The nonlinear magnetics including (cross-) saturation and all magnetic couplings are taken into account accurately. Optimization results are discussed which clearly show that a significant performance improvement is possible in comparison to existing methods. Differences in the resulting trajectories for low and high speed operation are investigated. From the results valuable insight is derived that can be used to improve the performance of real time capable EESM control algorithms.**

***Index Terms*—electrically excited synchronous machine, wound rotor synchronous machine, optimal control, non-linear control**

I. Introduction

To maximize the dynamics of a drive system the torque control loop must be optimized to track the set value as fast as possible. This improves the performance in motion control during changing set values and for increased immunity against external disturbances. Increasing the torque-dynamic has therefore always been a focus of research [1], [2].

In recent years the interest in electrically excited synchronous machines (EESM) and their control systems has increased especially for the use in electric vehicles (EV). The EESM provides high power density, efficiency and safety. It does not rely on rare earth magnets and thus eliminates supply-chain risks.

In an EESM the rotor flux can be controlled by adjusting the excitation current i_e. Compared to the permanent magnet synchronous machine (PMSM) this results in an additional degree of freedom. While the PMSM is modeled in a two-dimensional state space with the state variables $(i_\mathrm{d}, i_\mathrm{q})$, the state space of the EESM is three-dimensional with $(i_\mathrm{d}, i_\mathrm{q}, i_\mathrm{e})$. The additional component increases the complexity of torque control.

A. State of the Art Methods

In most approaches the torque control loop is composed of two parts [3]–[7]. First an operating point controller (OPC) is used to map the set torque to corresponding current values which are subsequently set by a closed-loop current controller.

The OPC is required as a given torque can be reached at different points in the three-dimensional state space. All points with identical torque form a curved surface. The task of the OPC is to select an operating point from the corresponding torque surface. Strategies that optimize for steady state efficiency have been investigated [3]–[7]. As a result of the optimization the excitation current needs to be adjusted in dependence of set torque and machine speed.

One special challenge in highly dynamic closed-loop current controllers for EESMs is the magnetic coupling between the d- and e-axis. The strong nonlinear magnetics present in highly utilized EESMs for EVs amplify the complexity of the control problem. Model predictive approaches have been proposed [8] which employ non-linear flux models in form of flux maps. In [9], a non-linear PI-controller is used with a decoupling technique based on a magnetic equivalent circuit. Both approaches have been shown to be fast and accurate but are fundamentally limited by the available voltage.

In proposed designs for use in EVs the exciter current is reduced by using a large exciter inductance - often magnitudes larger than the stator inductances [4], [6], [7], [10]. This causes the exciter dynamics to be much slower compered to the stator even when the controller is operating on the voltage limit. The combination of the efficiency optimized OPC and the low exciter dynamic lead to a reduced torque dynamic. To mitigate

$$\underbrace{\begin{pmatrix}\dot{\psi}_\mathrm{d}\\ \dot{\psi}_\mathrm{q}\\ \dot{\psi}_\mathrm{e}\end{pmatrix}}_{\underline{\dot{\psi}}} = -\underbrace{\begin{pmatrix}R_\mathrm{s} & 0 & 0\\ 0 & R_\mathrm{s} & 0\\ 0 & 0 & R_\mathrm{e}\end{pmatrix}}_{\underline{M}_\mathrm{R}} \cdot \underbrace{\begin{pmatrix}i_\mathrm{d}\\ i_\mathrm{q}\\ i_\mathrm{e}\end{pmatrix}}_{\underline{i}} - \underbrace{\begin{pmatrix}0 & -\omega & 0\\ \omega & 0 & 0\\ 0 & 0 & 0\end{pmatrix}}_{\underline{M}_\omega} \cdot \underbrace{\begin{pmatrix}\psi_\mathrm{d}\\ \psi_\mathrm{q}\\ \psi_\mathrm{e}\end{pmatrix}}_{\underline{\psi}} + \underbrace{\begin{pmatrix}v_\mathrm{d}\\ v_\mathrm{q}\\ v_\mathrm{e}\end{pmatrix}}_{\underline{v}} \tag{4}$$

this effect [6] proposed a method based on choosing optimal d- and q-current values for a slowly changing exciter-current.

While time optimal control regarding torque and flux has been studied extensively for permanent magnet synchronous machines [1], [2] there are no equivalent analyses for EESMs.

B. Contribution of this Work

The goal of this paper is to analyze how the EESM is controlled best to mitigate the limited rotor dynamics and achieve an optimal torque response while still maintaining optimal steady state efficiency. For this the optimal control problem (OCP) is formulated and solved numerically. In the presented method no simplifications in the system dynamics is needed, all nonlinearities of the EESM are taken into account and the approach can be used in the whole operating range. Solving the OCP requires computing power that is not available in real-time operation though. Therefore the optimal results are analyzed and key concepts are derived. These enable the development of operating schemes that replicate the optimal control trajectories in real time systems.

This work starts by introducing the drive system including the nonlinear EESM model in section II. In section III the method used to calculate steady state operating points is introduced before the formulation of the OCP is motivated in section IV. The Problem is solved by employing methods of dynamic optimization. In section V the optimization results for low speed operation are discussed and key principles of a time optimal operating scheme are derived. Subsequently, optimization results for high speed operation are presented.

II. Model of the EESM Drives System

In this work the drive system consists of an EESM which is fed by voltage source inverters in stator and rotor.

A. Non-Linear Machine Model in Rotor Orientation

The stator voltage equations of a three phase synchronous machine in rotor orientation are obtained by applying Clarke- and Park-transformation to the phase voltage equations.

$$v_\mathrm{d} = R_\mathrm{s} i_\mathrm{d} + \dot{\psi}_\mathrm{d} - \omega\psi_\mathrm{q} \tag{1}$$

$$v_\mathrm{q} = R_\mathrm{s} i_\mathrm{q} + \dot{\psi}_\mathrm{q} + \omega\psi_\mathrm{d} \tag{2}$$

For the EESM the exiter voltage equation is given by

$$v_\mathrm{e} = R_\mathrm{e} i_\mathrm{e} + \dot{\psi}_\mathrm{e} \tag{3}$$

In the above equations ψ_x are the flux, i_x the current and v_x the voltage components for stator d- and q-axis and exciter respectively. The resistance of stator and exciter are R_s and R_e and ω is the electrical frequency. The system can be written as a state space model in matrix vector notation as shown in (4). In this form the flux $\underline{\psi}$ can be seen as the three-dimensional state vector and $\underline{v}$ as the input.

The nonlinear magnetics including all couplings, saturation and cross-saturation are fully modeled using a three-dimensional flux map

$$f_\psi : \underline{i} \mapsto \underline{\psi} \tag{5}$$

which can be determined by finite element analysis or measurement. An excerpt of an EESM flux map is shown in fig. 1.

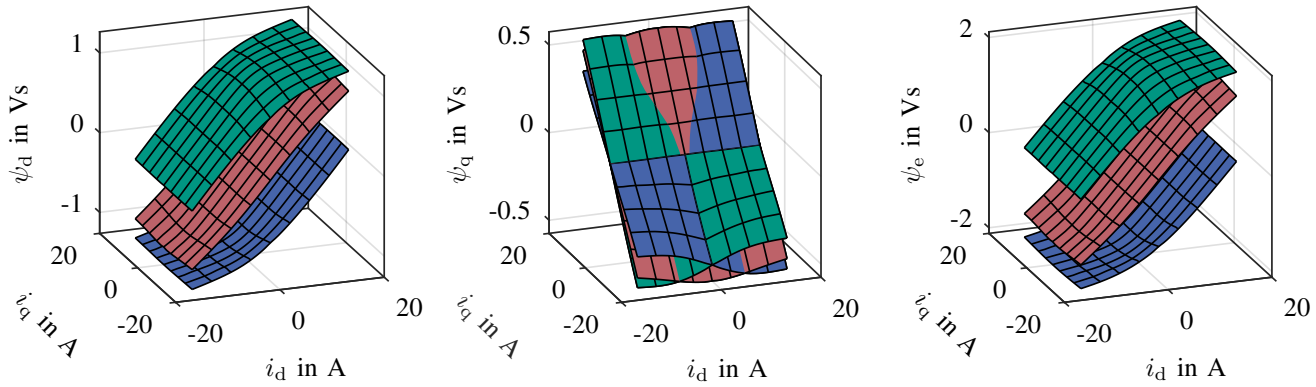

Fig. 1. Excerpt of an EESM flux map for $i_\mathrm{e} = -11$ A (blue), $i_\mathrm{e} = 0$ A (red) and $i_\mathrm{e} = 11$ A (green)

The associated machine has been designed in [11] and is used in this work. The corresponding inverse flux map

$$f_{\underline{\psi}}^{-1} : \underline{\psi} \mapsto \underline{i} \tag{6}$$

can be calculated as described in [12]. As mapping between current and flux is possible in both directions a formulation of (4) with the currents as the state vector is possible and mathematically equivalent.

With the number of pole pairs p the machine torque is calculated by (7).

$$T = \frac{3}{2} p(\psi_\mathrm{d} i_\mathrm{q} - \psi_\mathrm{q} i_\mathrm{d}) \tag{7}$$

Note that ψ_d predominantly depends on both the d- and e-current component due to magnetic coupling.

B. Inverter

The stator voltages are set by a two-level, three-phase inverter. To reduce complexity the stator voltage limit is modeled as

$$||(v_\mathrm{d}, v_\mathrm{q})|| \leq \frac{v_\mathrm{DC}}{\sqrt{3}} = v_\mathrm{s,max} \tag{8}$$

Dynamic overmodulation can be included in the following methods by modifying the voltage limit but will lead to results that depend on the rotor angle position as shown in [2] for a PMSM. As the dynamic is mostly limited by the exciter this simplification only has minor effects on the overall result.

In this work the exciter is operated by a single-phase, full-bridge inverter which results in a voltage limit of

$$|v_\mathrm{e}| \leq v_\mathrm{DC} = v_\mathrm{e,max} \tag{9}$$

Note that in some designs different intermediate circuits are used for stator and exciter. Also depending on the exciter design its voltage limit may not be symmetric. The methods proposed in the following can easily be adjusted to account for these differences.

III. Steady State Operating Points

In this work the operating points with the lowest ohmic losses are selected for steady state operation as proposed in [4]. For this the nonlinear optimization problem

$$\underline{i}_\mathrm{stat} = \underset{\underline{i}}{\operatorname{argmin}} \frac{3}{2} R_\mathrm{s}(i_\mathrm{d}^2 + i_\mathrm{q}^2) + R_\mathrm{e} i_\mathrm{e}^2 \tag{10}$$

$$s.t. \qquad T(\underline{i}) = T^* \tag{11}$$

$$i_\mathrm{d}^2 + i_\mathrm{q}^2 \leq i_\mathrm{s,max}^2 \tag{12}$$

$$i_\mathrm{e} \leq i_\mathrm{e,max} \tag{13}$$

$$0 \leq i_\mathrm{e} \tag{14}$$

$$v_\mathrm{d}(\underline{i}, \omega)^2 + v_\mathrm{q}(\underline{i}, \omega)^2 \leq v_\mathrm{s,max}^2 \tag{15}$$

is solved numerically to obtain the current set values $\underline{i}_\mathrm{stat}$ for set torque T^* at speed ω. Due to symmetry in the flux map every torque value can be reached with a positive or a negative exciter current. To get a unique solution only positive exciter currents are allowed. The stator voltages are calculated using (1) and (2) for steady state operation and the torque is calculated by (7). Note that both calculations require the use of the flux map. A constraint that enforces the exciter voltage limit is not needed in steady state operation if $R_\mathrm{e} i_\mathrm{e,max} \leq v_\mathrm{e,max}$ is satisfied. The optimization is solved for a grid of torque and speed values in the whole operating range. For use in a controller the results are stored in a lookup table (LUT). The maximum efficiency steady state operating points in base speed operation for the EESM [11] are shown in current and flux space in fig. 2 and fig. 3. Machine data and the operating limits used are given in tab. I.

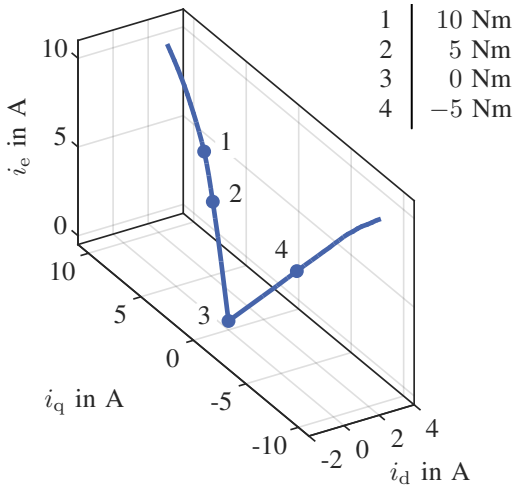

Fig. 2. Steady state operating points for base speed operation in current space

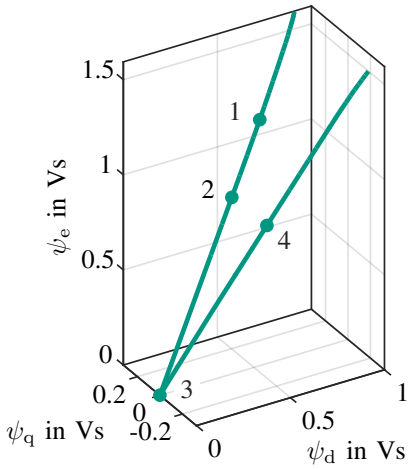

Fig. 3. Steady state operating points for base speed operation in flux space

IV. The Optimal Control Problem

The following analysis is carried out using the state space model (4) and the flux components as the state vector.

A. Definition of the Optimal Control Problem

A state transition from an initial starting point $\underline{\psi}_\mathrm{S}$ to a target point is characterized by its trajectory in state space which is written as

$$\underline{\psi}(t) \quad \text{with} \quad \underline{\psi}(0) = \underline{\psi}_\mathrm{S} \tag{16}$$

TABLE I
CHARACTERISTIC DATA OF THE EESM

Symbol	Meaning	Value
$P_{\max}$	maximum Power	5.9 kW
$i_{\mathrm{s,max}}$	maximum stator current	13 A
$i_{\mathrm{e,max}}$	maximum excitation current	10 A
$v_{\mathrm{s,DC}}$	stator DC link voltage	400 V
$v_{\mathrm{e,DC}}$	exciter DC link voltage	20 V
R_{e}	exciter resistance	$1.44\,\Omega$

The optimal state trajectory to the stationary operating point $\underline{\psi}_{\mathrm{stat}} = f_{\psi}^{-1}(\underline{i}_{\mathrm{stat}})$ for set torque T^* and a given speed ω is to be calculated.

It is possible to minimize the time until T^* is reached which is limited by how fast the exciter flux can be build up. Many trajectories exist that can reach T^* in almost identical time but differ greatly in their course in the stator flux variables and thus also in the torque along the trajectory. Of these many trajectories the one that increases the torque towards the set value the quickest is preferred. Thus the objective of the optimization in this work is to minimize the torque-time-area

$$\min_{\underline{\psi}(t)} \int_0^{t_{\mathrm{e}}} \Delta T(\underline{\psi}(\tau))\mathrm{d}\tau \tag{17}$$

with $\Delta T(\underline{\psi}) = |T(\underline{\psi}) - T^*|$.

In this form the endpoint is not specified and thus the resulting trajectory will lead to a point in the T^*-surface that can be reached fast. To get a trajectory that leads to the stationary operating point a secondary objective has to be included in the objective function. This is done by adding the flux-time-area with $\Delta\psi(t) = ||\underline{\psi}(t) - \underline{\psi}^*||$ to the function:

$$\min_{\underline{\psi}(t)} \int_0^{t_{\mathrm{e}}} \Delta T(\underline{\psi}(\tau)) + S \cdot \Delta\psi(\tau)\mathrm{d}\tau \tag{18}$$

To make sure the influence of the flux-time-area on the torque characteristic is negligible the scaling factor S has to be set to a sufficiently small value. In this work S is chosen so that the share of the flux-time-area is a least three orders of magnitude smaller than the one of the torque-time-area.

The inequality constraints

$$i_{\mathrm{d}}(\underline{\psi}(t))^2 + i_{\mathrm{q}}(\underline{\psi}(t))^2 \leq i_{\mathrm{s,max}}^2 \tag{19}$$
$$i_{\mathrm{e}}(\underline{\psi}(t))^2 \leq i_{\mathrm{e,max}}^2 \tag{20}$$
$$v_{\mathrm{d}}(\underline{\psi}(t))^2 + v_{\mathrm{q}}(\underline{\psi}(t))^2 \leq v_{\mathrm{s,max}}^2 \tag{21}$$
$$v_{\mathrm{e}}(\underline{\psi}(t))^2 \leq v_{\mathrm{e,max}}^2 \tag{22}$$

ensure that the trajectory stays within the current and voltage limits at any point in time.

B. Solution Method for the Dynamic Optimization Problem

In this work a direct approach is used in which the dynamic optimization problem is transcribed to a parameter optimization problem [13]. This has the advantage that all nonlinear constraints for the state variables can be included easily. The resulting parameter optimization problem can be solved using a nonlinear parameter optimization solver.

The state trajectory is discretized with $N+1$ points equidistantly with time increment Δt:

$$\underline{\psi}_n = \underline{\psi}(n\Delta t)\,, \quad n = 0 \cdots N \tag{23}$$
$$\underline{\psi}_0 = \underline{\psi}_{\mathrm{S}} \tag{24}$$

The objective function is discretized using the trapezoidal rule:

$$\min_{\underline{\psi}_1 \cdots \underline{\psi}_{\mathrm{N}}} A_{\mathrm{T}}(\underline{\psi}_1 \cdots \underline{\psi}_{\mathrm{N}}) + S \cdot A_{\psi}(\underline{\psi}_1 \cdots \underline{\psi}_{\mathrm{N}}) \tag{25}$$

$$A_{\mathrm{T}}(\underline{\psi}_1 \cdots \underline{\psi}_{\mathrm{N}}) = \sum_{k=0}^{N-1} \frac{\Delta t}{2}(\Delta T(\underline{\psi}_k) + \Delta T(\underline{\psi}_{k+1})) \tag{26}$$

$$A_{\psi}(\underline{\psi}_1 \cdots \underline{\psi}_{\mathrm{N}}) = \sum_{k=0}^{N-1} \frac{\Delta t}{2}(\Delta\psi(\underline{\psi}_k) + \Delta\psi(\underline{\psi}_{k+1})) \tag{27}$$

As the starting point of the trajectory is given, the elements of the remaining flux vectors $\underline{\psi}_1 \cdots \underline{\psi}_{\mathrm{N}}$ are the $3N$ decision variables of the optimization problem.

To ensure that the trajectory is compatible with the system dynamics, the differential equation (4) is discretized using the trapezoidal rule.

$$\underline{v}_k = \underline{M}_{\mathrm{R}} \frac{\underline{i}_{k-1} + \underline{i}_k}{2} + \frac{\underline{\psi}_k - \underline{\psi}_{k-1}}{\Delta t} + \underline{M}_{\omega} \frac{\underline{\psi}_{k-1} + \underline{\psi}_k}{2} \tag{28}$$

The voltage is modeled as constant between two consecutive flux points which reflects the behavior of the switching inverter that sets a mean voltage over one modulation period. The $\underline{i}_x$ are given by $\underline{i}_x = f_{\psi}^{-1}(\underline{\psi}_x)$. Thus the system dynamics is respected if the voltages $\underline{v}_k$ stay within the operating limits. Together with the current limit this results in the nonlinear inequality constraints (29) to (32).

$$v_{\mathrm{d},k}^2 + v_{\mathrm{q},k}^2 \leq v_{\mathrm{s,max}}^2 \tag{29}$$
$$v_{\mathrm{e},k}^2 \leq v_{\mathrm{e,max}}^2 \tag{30}$$
$$i_{\mathrm{d},k}^2 + i_{\mathrm{q},k}^2 \leq i_{\mathrm{s,max}}^2 \tag{31}$$
$$i_{\mathrm{e},k}^2 \leq i_{\mathrm{e,max}}^2 \tag{32}$$

These have to be fulfilled for $k = 1 \cdots N$ which leads to $4N$ constraints in total.

V. OPTIMIZATION RESULTS

A. Data Set and Solution Setup

The following results are produced using the data set of the EESM [11] with the data in tab. I and the flux maps in fig. 1. Steady state operating points used are marked in fig. 2 and 3.

Compared to the reference designs [4], [6], [7], [10] the exciter of the prototype has a much lower number of windings. The exciter flux-linkage is accordingly smaller. Thus stator and exciter flux-linkage are in the same order of magnitude and the dynamics of both will be similar if operated with the same DC link voltage. To emulate the behavior of a machine with limited rotor dynamics the exciter voltage limit is decreased. This has the same effect on the exciter dynamics as rewinding the rotor with a higher winding number. The value of the reduction factor is chosen to match the ratio of stator to exciter flux linkage in the reference designs. Therefore the machine

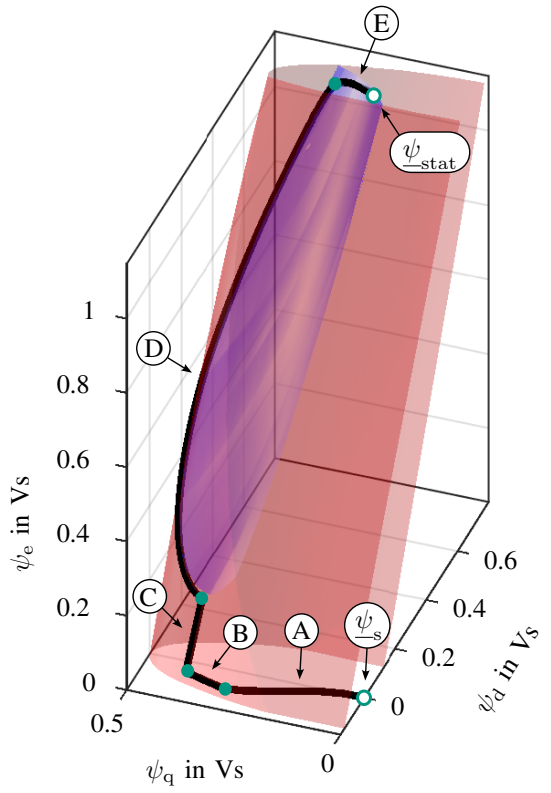

Fig. 4. optimal trajectory (black), T^*-surface (blue), current limit (red)

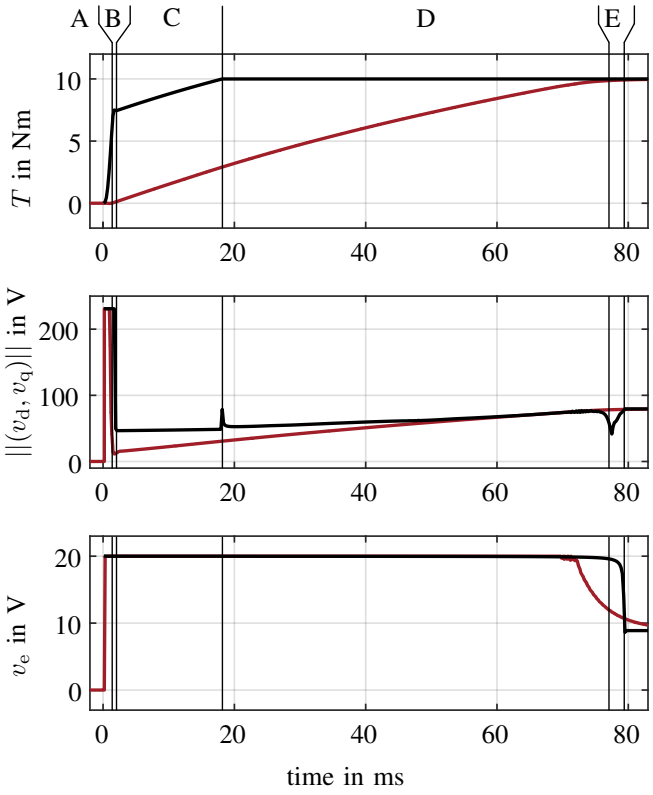

Fig. 6. Torque and voltage - optimization(black), reference controller (red)

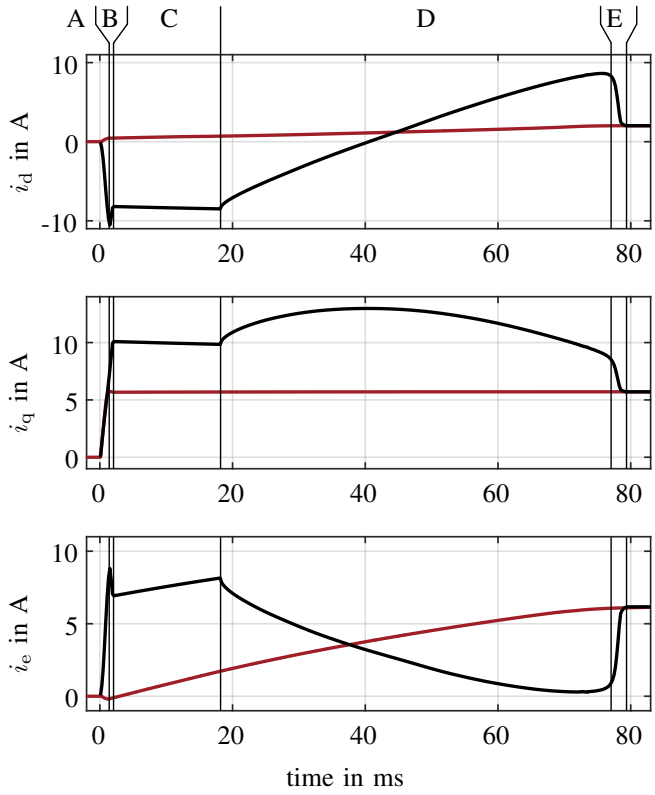

Fig. 5. Current - optimization (black), reference controller (red)

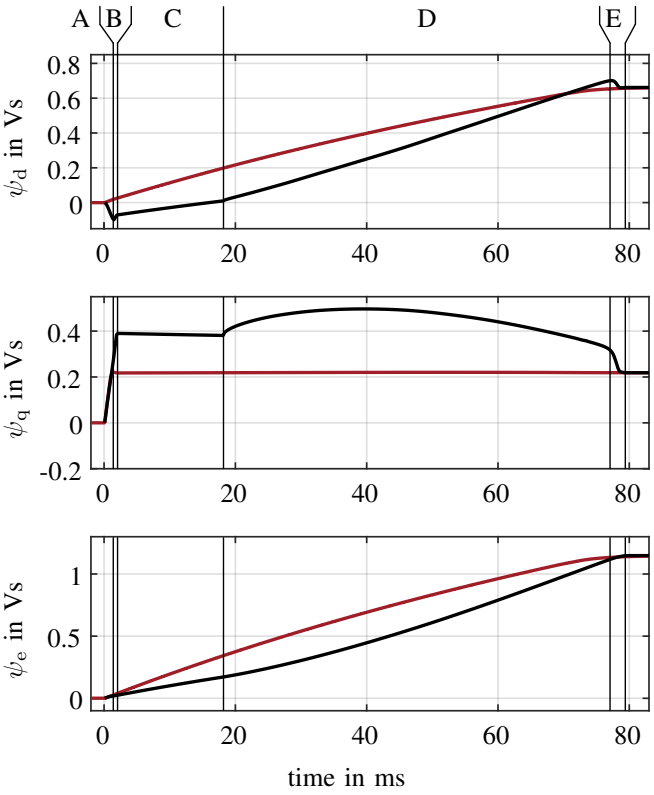

Fig. 7. Flux - optimization (black), reference controller (red)

is operated with the low exciter DC link voltage of 20V. As the exciter is connected to a full-bridge inverter by slip rings positive and negative voltages can be applied.

In this work the function "fmincon" from MATLAB's Optimization Toolbox is used to solve the optimization problem (25). The trajectories are discretized with a time step of $\Delta t = 200\mu$s. The number of points is chosen depending on the length of the state transition.

B. Optimal Trajectories for Low Speed Operation

In this section the optimization result for a step response from 0 Nm to 10 Nm at 500 rpm is presented. In fig. 4 the optimal trajectory is shown in flux space. Time courses of torque, current, flux and voltage are shown in fig. 5-7 for the optimization result and for the PI-controller [9] under the same boundary conditions. The possible performance improvement regarding torque dynamics is clearly visible.

The optimal trajectory can be divided in five parts denoted A-E. As expected $v_\mathrm{e} = v_\mathrm{e,max}$ throughout the whole trajectory to build up exciter flux quickly. Thus the state point in flux space moves continuously upwards along the ψ_e-axis on the trajectory shown in fig. 4. In section A i_e is increased rapidly while i_d moves in the opposite direction. Here the effect of magnetic coupling is used. The linear approximation of the flux equation $\psi_\mathrm{e} = L_\mathrm{e} i_\mathrm{e} + M i_\mathrm{d}$ helps to illustrate this effect. While the dynamic of ψ_e is limited, the current components that build up the flux can be changed highly dynamic. Precondition is that they are changed in opposite directions to keep the rate of flux change within the voltage limit. By this principle, in A and B the stator flux can be steered to the point of maximum torque for the currently available exciter flux which is reached at the end of B. The change of direction at the end of A is because the stator current limit is reached and subsequently held during B, C and D. In C the exciter flux value is not sufficient to reach T^*. Therefore, the trajectory follows the line of maximum available torque until T^* is reached at the beginning of D. In D and E the trajectory continues in the T^*-surface toward $\underline{\psi}_\mathrm{stat}$. During D the flux point in the T^*-surface with the largest i_d and thus the smallest i_e is chosen. This reduces the ohmic voltage drop $R_\mathrm{e} i_\mathrm{e}$ in the exciter which in turn leaves a larger portion of the applied voltage for the exciter flux increase. Compared to the reference control method the ohmic voltage drop in the exciter is larger in the first half of the transition where the e-current is needed to produce torque and lower in the second half. Thus in this example both methods reach the end point almost simultaneously. In the EESM designs [4] and [6] the ohmic voltage drop in the exciter is in the range of $25-70\%$ of $v_\mathrm{e,max}$. Using this effect to support the increase or decrease of ψ_e can thus be an effective measure to increase the exciter flux dynamic. As it seams counter intuitive to decrease the exciter current in order to increase its flux this is not used in existing methods. When target ψ_e is reached at the end of D the system is moved to $\underline{\psi}_\mathrm{stat}$ in part E for stationary operation.

C. Optimal Trajectories for High Speed Operation

With increasing speed the shape of the optimal trajectory changes. This becomes especially apparent in the field weakening region which start at 1000 rpm for the given machine. This is shown at the example of a step response from -5 Nm to 5 Nm. The optimal trajectories are calculated for low speed with 500 rpm and for high speed with 2000 rpm.

The torque values of ± 5 Nm are well below the maximum torque and thus the optimization (10) results in the same stationary operating points for both speeds. The flux components of start and end point of the trajectory only differ in the flipped sign in the q-component.

The trajectories and the time needed to reach the end point differs greatly as can be seen in fig. 8 and fig. 10. The difference is rooted in the voltage component $\underline{M}_\omega \underline{\psi}$. By numeric integration of (4) over a time interval Δt for voltage vectors with $||(v_\mathrm{d}, v_\mathrm{q})|| = v_\mathrm{s,max}$ the region of flux point that can be reached in Δt from a given point is calculated. As the stator resistance is low the effect of the ohmic voltage drop is small. At low speeds the share of $\underline{M}_\omega \underline{\psi}$ is low too. The flux values in reach form a circle centered around the current state.

For low speeds the quickest path towards the set torque is thus simply the shortest path. This can be seen in the optimal trajectory that moves toward the closest point with T^* and continues afterwards in the T^*-surface.

At high speeds the effect of the induced voltage increases and shift the circle of reachable flux points. The distance that can be covered in Δt now depends on the direction. On the straight line toward the T^*-surface only small steps can be made which leads to decreased dynamics. The optimization results in a path that is longer in space but that can be covered more quickly because is moves in directions where larger steps are possible. Fig. 9 shows a decrease in the exciter flux which at first seems to be inconsistent as the flux has to be build up again later. But in fact by decreasing the exciter flux larger steps in the direction of the T^*-surface are possible. After T^* is reached the path continues in the T^*-surface. Analogously to sec. V-B the system is moved to the largest ψ_d value which correlates to the largest i_d and in turn to the smallest i_e. This decreases ohmic voltage drop in the exciter and allows to build up the exciter flux again quickly.

Similar results in the high speed operating range have been described for time optimal control of the PMSM that can be considered a similar but less complex problem as the third dimension in the state space doesn't exist. For this case, trajectories that are similarly curved in the d-q-plane have been reported in [2]. The two-dimensional optimal control problem is also analyzed in [1] in the stationary reference frame. Here it is found that the optimal trajectory can also be described as a straight line towards a rotating target point. The curvature can be interpreted as a result of the Park-transform. Due to the additional coupling with the exciter component the problem in this work is more complex. However similar observations can be found in literature and can help to better understand the optimal dynamics of the EESM.

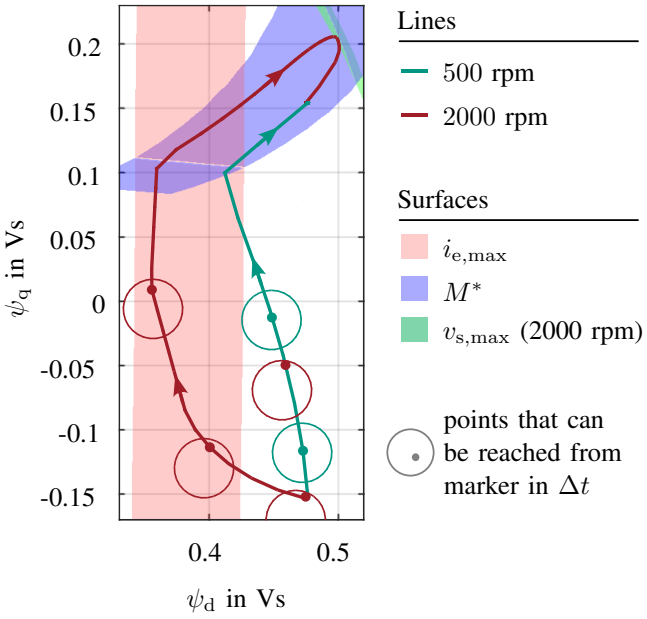

Fig. 8. Trajectories in ψ_d-ψ_q-plane

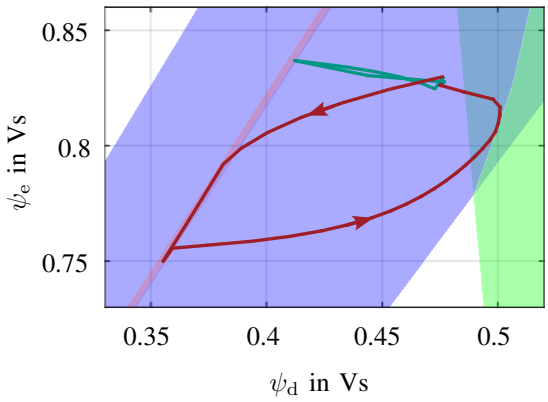

Fig. 9. Optimization results in ψ_d-ψ_e-plane (legend identical to fig. 8)

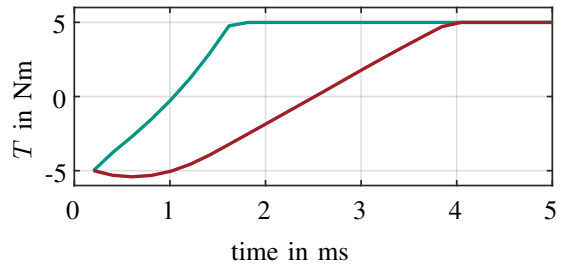

Fig. 10. Torque response from optimization at 500 rpm (green) and 2000 rpm (red)

VI. Conclusion and Outlook

In this work a method to calculate time optimal trajectories between maximum efficiency operating points for an EESM has been proposed. Optimization results for state transitions in the low and high speed operating range have been presented. The results show significant possible improvement compared to existing methods. Two key concepts have been identified: First, the magnetic coupling of d- and e-component can be used to change the rotor current quickly in order to reach an operation point with high torque faster. This will happen automatically if the operating point with highest torque at available exciter flux is selected. Second, the ohmic voltage drop in the exciter can be used to change the rotor flux faster. These two concepts can be used to improve the control dynamic of EESM drive systems. For high speed operation the complexity of the optimal trajectories increases due to curvature. The insights derived from the analysis of time optimal control trajectories in this work can be used to mitigate the problem of limited rotor dynamic in EESM drive systems while still maintaining optimal steady state efficiency.

References

[1] J.-W. Choi and S.-K. Sul, "Generalized solution of minimum time current control in three-phase balanced systems," *IEEE Transactions on Industrial Electronics*, vol. 45, no. 5, pp. 738–744.

[2] A. Brosch, O. Wallscheid, and J. Böcker, "Time-optimal model predictive control of permanent magnet synchronous motors considering current and torque constraints," *IEEE Transactions on Power Electronics*, vol. 38, no. 7, pp. 7945–7957, 2023.

[3] M. Märgner and W. Hackmann, "Control challenges of an externally excited synchronous machine in an automotive traction drive application," in *2010 Emobility - Electrical Power Train*, 2010, pp. 1–6.

[4] O. Haala, B. Wagner, M. Hofmann, and M. Marz, "Optimal current control of externally excited synchronous machines in automotive traction drive applications," *International Journal of Electrical and Computer Engineering*, vol. 7, no. 9, pp. 1133 – 1139, 2013.

[5] J. Reinhard, K. Löhe, and K. Graichen, "Optimal current setpoint computation for externally excited synchronous machines," in *2022 IEEE Conference on Control Technology and Applications (CCTA)*, 2022, pp. 1319–1326.

[6] R. Breda, G. Andrioli, S. Calligaro, and R. Petrella, "Extended mtpa and flux-weakening control with total copper loss minimisation and transient torque compensation for wound-rotor synchronous machines," in *2023 IEEE ECCE*, 2023, pp. 4829–4836.

[7] Y. Kim and K. Nam, "Copper-loss-minimizing field current control scheme for wound synchronous machines," *IEEE Transactions on Power Electronics*, vol. 32, no. 2, pp. 1335–1345.

[8] J. Stoß, L. Geier, A. Karayel, S. Decker, A. Liske, and M. Hiller, "Unified predictive flux control for eesm, im, pmsm and syrm," in *2023 IEEE Energy Conversion Congress and Exposition (ECCE)*, 2023, pp. 5009–5019.

[9] S. Goehner, J. Stoss, M. Brodatzki, B. Bachowsky, A. Liske, J. Kolb, and M. Hiller, "New current control strategy for eesms based on the magnetic equivalent circuit with dynamic decoupling of the d- and e-axis," in *2023 IEEE 8th SPEC/COBEP*, 2023, pp. 1–8.

[10] J. Tang and Y. Liu, "Design of electrically excited synchronous machines to achieve unity power factor in field weakening for long-haul electric trucks," in *2020 International Conference on Electrical Machines (ICEM)*, vol. 1, 2020, pp. 422–428.

[11] P. Winzer, "Steigerung von drehmoment und wirkungsgrad bei synchronmaschinen durch nutzung der magnetischen asymmetrie," Ph.D. dissertation, Karlsruher Institut für Technologie (KIT), 2017.

[12] L. Geier, J. Stoß, A. Liske, and M. Hiller, "Generalized inversion of n-dimensional flux maps for unified nonlinear machine models and predictive control algorithms," in *2023 IEEE Energy Conversion Congress and Exposition (ECCE)*, 2023, pp. 4821–4828.

[13] J. T. Betts, *Practical Methods for Optimal Control and Estimation Using Nonlinear Programming, Second Edition*, 2nd ed. Society for Industrial and Applied Mathematics, 2010.